IEEE Access
Multidisciplinary | Rapid Review | Open Access Journal

Received 24 December 2022, accepted 31 December 2022, date of publication 3 January 2023, date of current version 9 January 2023.

Digital Object Identifier 10.1109/ACCESS.2022.3233941

RESEARCH ARTICLE

Coded Assisted Transmit and Receive IQ Mismatch Compensation With Channel Estimation for AF Cooperative OFDM Systems

MOHAMED MAREY[1], (Senior Member, IEEE), AND HALA MOSTAFA[2], (Member, IEEE)
[1]Smart Systems Engineering Laboratory, College of Engineering, Prince Sultan University, Riyadh 11586, Saudi Arabia
[2]Department of Information Technology, College of Computer and Information Sciences, Princess Nourah bint Abdulrahman University, Riyadh 11671, Saudi Arabia

Corresponding author: Hala Mostafa (HFMostafa@pnu.edu.sa)

Princess Nourah bint Abdulrahman University Researchers Supporting Project number (PNURSP2023R137), Princess Nourah bint Abdulrahman University, Riyadh, Saudi Arabia.

ABSTRACT Amplify-and-forward (AF) orthogonal frequency division multiplexing (OFDM) transmissions encounter a significant difficulty in the form of in-phase and quadrature phase (IQ) mismatch. Previous reports on this problem have solely been discussed in the context of uncoded transmissions. In addition, in these precedent studies, IQ equalization must be conducted following the estimation stage for accurate detection of data symbols. This research delves into the issue of the IQ mismatch between transmission and reception in AF-OFDM systems in the context of channel coding. We design a magnificent code-aided approach to predict the overall channel impulse responses (CIRs), which encompass the actual CIRs and IQ mismatch originating at the source, relay, and destination. Instead of using a collection of algorithms, the proposed approach can be utilized to estimate nine parameters simultaneously. Due to the impractical nature of the precise maximum-likelihood (ML) strategy to this situation, we instead utilize an expectation-maximization (EM) process as a low complexity strategy to predict the parameters under consideration. The suggested estimation approach uses an iterative process to improve predictions exploiting the *a priori* knowledge gained from the soft information supplied by the channel decoder. In addition, we demonstrate how to carry out data detection by making use of the estimated parameters. The simulation results verify the effectiveness of the proposed estimator and detector for usage in real-world settings, with superiority over the conventional ones.

INDEX TERMS OFDM, IQ mismatch, cooperative transmissions.

I. INTRODUCTION

Orthogonal frequency division multiplexing (OFDM) has emerged as the strategy of choice for current and next-generation wireless standards due to its reliability in frequency-selective multipath circumstances and high spectrum efficiency utilization [1], [2]. It has been considered for use in the settings of cellular networks, including the fifth-generation and beyond systems, with its deployment in long term evolution standards [3], [4], [5]. It has also been effectively deployed in a wide range of other wireless technologies, including local area networks, and radars, microwave, and satellite systems [6], [7], [8].

Direct conversion technology has seen widespread use in the telecommunications industry due to its minimal complication and expense [9]. Unfortunately, it causes restrictions such as inphase (I) /quadrature (Q) phase (IQ) mismatch, which translates to a significant drop in data delivery [10], [11]. When compared to the ideal condition, in which the sine and cosine branches have a precise 90 degree phase shift and identical amplitude, the IQ mismatch is essentially the discrepancy between the I and Q branches. Furthermore, the IQ mismatch illustrates the imperfections of the other analog parts, such as analog filters, amplifiers, mixers, and digital-to-analog converters, which

The associate editor coordinating the review of this manuscript and approving it for publication was Pinjia Zhang.

This work is licensed under a Creative Commons Attribution 4.0 License. For more information, see https://creativecommons.org/licenses/by/4.0/

are deployed in two branches of a transceiver. This disparity is associated with analog processing due to component defects that are neither predictable nor tunable, and are expected to increase as production volumes decrease. It is important to keep in mind that perfect IQ matching is not attainable, particularly when easy fabrication technologies are employed. More bandwidth and higher carrier frequencies being used in modern communication systems increase IQ disparities. OFDM systems are more susceptible to the IQ discrepancy than single-carrier systems because of the spectral overlap between the subcarriers. As a consequence of the IQ mismatch issue, sub-carrier orthogonality is lost, which in turn causes inter-carrier interference and a significant drop in performance [12], [13]. There is a wealth of literature on the topic of the impact, estimate, and correction of IQ mismatch for non-cooperative OFDM transmissions, see e.g., [14] and references therein.

In the meanwhile, wireless networks are increasingly turning to cooperative communications to boost throughput and/or dependability [15], [16]. This is facilitated with the assistance of one or more relaying nodes, which allow a source to deliver data to its intended recipient. The destination node arrives at a conclusion by appropriately integrating the signals that it has received from the source and the relays. Amplify-and-Forward (AF) and Decode-and-Forward (DF) are the two most common techniques that are used by relaying terminals [17]. When using AF, each relay in the system basically transmits to the destination a scaled version of the signals it has received, which includes both the information and the noise. The relay in a DF cooperative system first decodes the incoming signals, then re-encodes them for transmission.

Because each of OFDM and cooperative technologies has been demonstrated to be advantageous and effective on its own, their combination is a highly hot research topic that has recently been explored in a series of studies [18], [19], [20]. However, the integrated system also takes on the challenges that were faced by the individual systems. Without a doubt, the IQ mismatch is one of the primary issues that has to be addressed in order to ensure the transmission's reliability and effectiveness. Several distinct types of OFDM cooperative systems have been investigated regarding their outage performance in the presence of IQ mismatches [21], [22]. Within the context of a full-duplex OFDM relay system, an investigation into a least-square channel estimator with IQ mismatch has been carried out [23]. It was suggested in [24] that AF-OFDM systems benefit from a pilot-based IQ discrepancy compensating technique. At a relay node, the effectiveness of dual-hop and two-way relaying has been investigated when an IQ discrepancy is present [25], [26]. For DF two-path successive relaying OFDM systems, joint maximum-likelihood (ML) IQ mismatch correction and channel estimation techniques have been created [27], [28].

The following points are highlighted the predominant contributions of this article.

- We offer a comprehensive code-aided approach to jointly estimate the channel impulse responses (CIRs) and IQ mismatch arising at all nodes for AF-OFDM transmissions. This is in contrast to the standard practice, which involves a variety of approaches for estimating CIR between nodes and calculating the IQ mismatch that exists at each node.
- Overall CIRs are constructed by integrating the IQ effects at each node to the physical CIRs, resulting in two parameters that are evaluated by a ML approach.
- We make use of an expectation-maximization (EM) procedure [29], [30] to put the proposed ML strategy into action. For this purpose, the proposed estimate algorithm iteratively utilizes the *a posterior* probabilities of the sent bits offered by a channel decoder to calculate the *a posterior* expectations of the broadcast symbols.
- We demonstrate how the decoding procedure is carried out while the overall CIRs are being estimated.

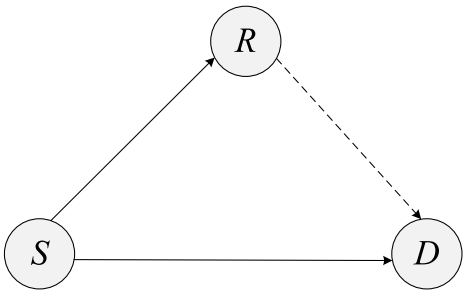

FIGURE 1. Cooperative system consists of three nodes. The solid line indicates the broadcast of the first time slot while the dashed line represents the transmission of the second time slot.

The following outline describes how the subsequent sections of the work are organized. The model of the AF-OFDM system that is being considered is described in Section II. Section III provides the proposed estimate technique, while Section IV covers the proposed data detection scheme. Simulation outcomes, as well as suitable analysis, are included in Section V. Finally, the research is wrapped up in Section VI.

II. SYSTEM DESCRIPTION

Our focus is on a cooperative OFDM system with three terminals: the source (S), the relay (R), and the destination (D) as displayed in Figure 1. The fundamental structure of each terminal is shown in figure 2. The relay incorporates an AF relaying technique and acts in a half-duplex mode, implying that transmission and reception take place at separate periods. A frame-based mode of transmission is assumed, wherein M OFDM symbols make up a frame. With the guidance of an error-correcting code, the source transforms a sequence of B information bits into C coded bits. These encoded bits are first interleaved, and then, with the assistance of a digital modulator, they are transformed into a series of Q symbols. Each symbol belongs to a signal constellation Ω, $Q = C/\log_2 \langle\Omega\rangle$, where $\langle\Omega\rangle$ refers to the cardinality of Ω. The entire data symbols are separated into M blocks, each with $N = Q/M$ data symbols. These blocks are placed in a buffer before being transformed to OFDM symbols one by one. Denoting ν as the cyclic prefix length, the nth sample of

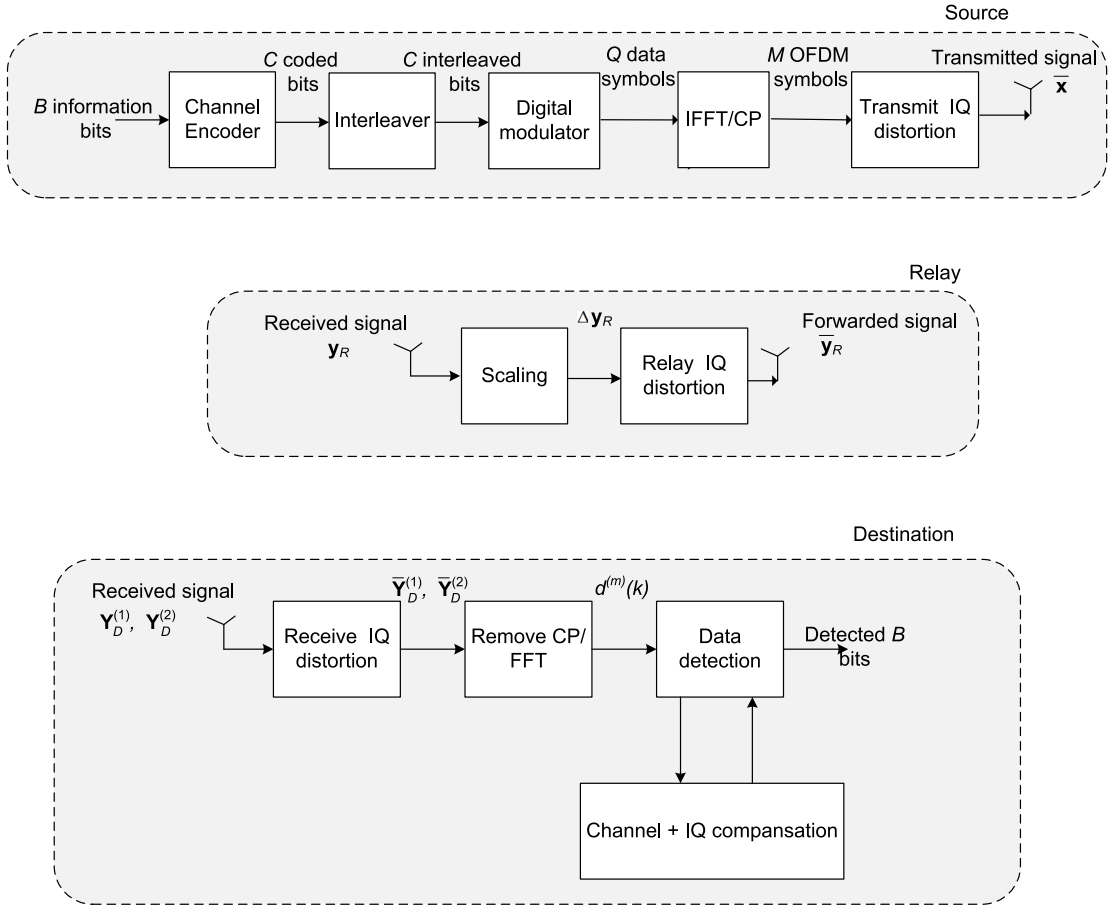

FIGURE 2. Fundamental structure of the source, relay, and destination.

the mth OFDM symbol is expressed as

$$x^{(m)}(n) = \frac{1}{\sqrt{N}} \sum_{k=0}^{N-1} d^{(m)}(k) \exp\left(-j2\pi nk/N\right), \quad (1)$$

where $n = 0, \cdots, N+\nu-1$, $d^{(m)}(k)$ is the kth data symbol of the mth OFDM symbol, and $j = \sqrt{-1}$. In this sense, $\overrightarrow{\mathbf{x}} = \left[\mathbf{x}^{(0)}, \mathbf{x}^{(1)}, \cdots, \mathbf{x}^{(M-1)}\right]^{\dagger}$ stands for the unaltered transmitted frame where $\mathbf{x}^{(m)} = \left[x^{(m)}(0), x^{(m)}(1), \cdots, x^{(m)}(N+\nu-1)\right]$ is the mth OFDM symbol and the superscript $\dagger$ is the vector transpose operator.

We denote θ_S and ρ_S as the phase and amplitude discrepancies between I and Q paths at the source. Let $\Re\left(\overrightarrow{\mathbf{x}}\right)$ and $\Im\left(\overrightarrow{\mathbf{x}}\right)$ describe the real and imaginary components of vector $\overrightarrow{\mathbf{x}}$, $\overrightarrow{\mathbf{x}} = \Re\left(\overrightarrow{\mathbf{x}}\right) + j\Im\left(\overrightarrow{\mathbf{x}}\right)$, where $\Re\left(\overrightarrow{\mathbf{x}}\right)$ is sent via the I branch and $\Im\left(\overrightarrow{\mathbf{x}}\right)$ is broadcast through the Q branch. Bearing this in mind, the modulated signals carried across the I and Q branches are respectively denoted as [21]

$$\breve{\mathbf{x}}_{\mathrm{I}}(n) = \Re\left(\overrightarrow{\mathbf{x}}(n)\right)(1+\rho_S)\cos\left(2\pi f_c nT_s + \theta_S\right), \quad (2)$$

$$\breve{\mathbf{x}}_{\mathrm{Q}}(n) = \Im\left(\overrightarrow{\mathbf{x}}(n)\right)(1-\rho_S)\sin\left(2\pi f_c nT_s - \theta_S\right), \quad (3)$$

where $\overrightarrow{\mathbf{x}}(n)$ is the nth component of vector $\overrightarrow{\mathbf{x}}$, f_c is the carrier frequency, and T_s is the sampling time. Accordingly, the sent radio frequency signal is represented as

$$\overline{\mathbf{x}}_{RF} = \breve{\mathbf{x}}_{\mathrm{I}} + \breve{\mathbf{x}}_{\mathrm{Q}}. \quad (4)$$

A general expression for a radio frequency signal is [31]

$$\overline{\mathbf{x}}_{RF}(n) = \Re\left(\overline{\mathbf{x}}(n)\exp\left(j2\pi f_c nT_s\right)\right), \quad (5)$$

where $\overline{\mathbf{x}}(n)$ is the nth element of the baseband vector $\overline{\mathbf{x}}$. Using (2), (3), and (4) into (5), we obtain the baseband frame damaged by the IQ mismatch at the source as

$$\overline{\mathbf{x}} = \eta_S \overrightarrow{\mathbf{x}} + \mu_S \overrightarrow{\mathbf{x}}^{*}, \quad (6)$$

where $*$ refers to the complex-conjugate operator, and η_S and μ_S are defined as

$$\eta_S = \cos(\theta_S) + j\rho_S \sin(\theta_S), \quad (7)$$

$$\mu_S = \rho_S \cos(\theta_S) + j\sin(\theta_S). \quad (8)$$

The frame transfer is typically accomplished in two rounds. The initial transmission of frame $\overline{\mathbf{x}}$ involves using two separate channels to approach both the relay and the destination terminals simultaneously. We denote $\mathbf{g}_{SR} = [g_{SR}(0), \cdots, g_{SR}(G-1)]^{\dagger}$ and $\mathbf{g}_{SD} = \left[g_{SD}(0), \cdots, g_{SD}(G-1)\right]^{\dagger}$ as the CIRs that exist between S and R, and S and D, correspondingly, with G being the number of channel

paths. The frames received at the relay and destination are represented as

$$\mathbf{y}_R = \bar{\mathbf{x}} \otimes \mathbf{g}_{SR} + \mathbf{w}_R, \tag{9}$$
$$\mathbf{y}_D^{(1)} = \bar{\mathbf{x}} \otimes \mathbf{g}_{SD} + \mathbf{w}_D^{(1)}, \tag{10}$$

where $\otimes$ is the linear convolution operator, and $\mathbf{w}_R$ and $\mathbf{w}_D^{(1)}$ are the noise vector at the relay and destination terminals, respectively. Note that we add superscripts 1 and 2 to the signal received at the destination to highlight that the signal received at the first time slot is different from that at the second time slot, as described in (10) and (13). Given that the relay only receives in a single time slot, we can omit the superscript from the signal's representation in (9). Applying the effect of IQ mismatch on $\mathbf{y}_R$ and $\mathbf{y}_D^{(1)}$, we get

$$\bar{\mathbf{y}}_R = \eta_R \mathbf{y}_R + \mu_R \mathbf{y}_R^*, \tag{11}$$
$$\bar{\mathbf{y}}_D^{(1)} = \eta_D \mathbf{y}_D^{(1)} + \mu_D \mathbf{y}_D^{(1)*}, \tag{12}$$

where η_R, μ_R, η_D, and μ_D are defined as indicated in (7) and (8) with replacing S with R and D. It should be noted that η_R and μ_R incorporate the impacts of the relay's transmit and receive IQ settings. We highlight the fact that the implications of IQ factors at the source, relay, and destination are all taken into account, as shown in (6), (11), and (12).

In the second part of the transmission process, the relay sends back the modified version of the received signal to the destination node. The collected signal at the destination is provided as

$$\mathbf{y}_D^{(2)} = \Delta \bar{\mathbf{y}}_R \otimes \mathbf{g}_{RD} + \mathbf{w}_D^{(2)}, \tag{13}$$

where $\mathbf{g}_{RD} = [g_{RD}(0), \cdots, g_{RD}(G-1)]^\dagger$ is the CIR between R and D terminals, $\mathbf{w}_D^{(2)}$ is the corresponding noise vector, and Δ is the scaling parameter given as [32]

$$\Delta = \frac{1}{\sqrt{\sum_{l=0}^{G-1} |g_{SR}(l)|^2 + \sigma_n^2}}. \tag{14}$$

Here, σ_n^2 is the noise variance. The result of introducing the IQ mismatch impact to $\mathbf{y}_D^{(2)}$ is

$$\bar{\mathbf{y}}_D^{(2)} = \eta_D \mathbf{y}_D^{(2)} + \mu_D \mathbf{y}_D^{(2)*}. \tag{15}$$

The aim of this investigation is to develop a data detection algorithm while simultaneously estimating all unknown parameters of $\mathbf{g}_{SR}$, $\mathbf{g}_{SD}$, $\mathbf{g}_{RD}$, η_S, μ_S, η_R, μ_R, η_D, and μ_D.

III. PROPOSED EM ESTIMATION ALGORITHM

The receiver's principal responsibility is to retrieve the data delivered by the source using the observations of $\bar{\mathbf{y}}_D^{(1)}$ and $\bar{\mathbf{y}}_D^{(2)}$. Knowing the IQ parameters at the source, relay, and destination, as well as the CIRs between the various nodes, is obviously necessary. Reformulating the preceding equations allows us to arrive at a solution to the issue at hand. Using (6), (10), into (12), we describe $\bar{\mathbf{y}}_D^{(1)}$ as

$$\bar{\mathbf{y}}_D^{(1)} = \overrightarrow{\mathbf{x}} \otimes \mathbf{g}_{SD}^{(1)} + \overrightarrow{\mathbf{x}} \otimes \mathbf{g}_{SD}^{(2)} + \left(\overrightarrow{\mathbf{x}}\right)^* \otimes \mathbf{g}_{SD}^{(3)} + \left(\overrightarrow{\mathbf{x}}\right)^* \otimes \mathbf{g}_{SD}^{(4)} + \mathbf{w}_D^{(1)}, \tag{16}$$

where

$$\mathbf{g}_{SD}^{(1)} = \eta_D \eta_S \mathbf{g}_{SD}, \tag{17a}$$
$$\mathbf{g}_{SD}^{(2)} = \mu_D \mu_S^* \mathbf{g}_{SD}^*, \tag{17b}$$
$$\mathbf{g}_{SD}^{(3)} = \eta_D \eta_S^* \mathbf{g}_{SD}, \tag{17c}$$
$$\mathbf{g}_{SD}^{(4)} = \mu_D \mu_S^* \mathbf{g}_{SD}^*. \tag{17d}$$

When we take into consideration the fact that a convolution operator can be represented in the form of a matrix, we rewrite (16) as

$$\bar{\mathbf{y}}_D^{(1)} = \mathbf{X}\mathbf{g}_{SD}^{(1)} + \mathbf{X}\mathbf{g}_{SD}^{(2)} + \mathbf{X}^*\mathbf{g}_{SD}^{(3)} + \mathbf{X}^*\mathbf{g}_{SD}^{(4)} + \mathbf{w}_D^{(1)}, \tag{18}$$

where $\mathbf{X}$ is described as an $(q+G-1) \times (G-1)$ matrix created as

$$\mathbf{X} = \begin{bmatrix} x_0 & 0 & 0 & 0 & 0 \\ x_1 & x_0 & 0 & 0 & 0 \\ x_2 & x_1 & x_0 & 0 & 0 \\ \vdots & \vdots & \vdots & \vdots & \vdots \\ x_q & x_{q-1} & x_{q-2} & \cdots & x_{q-G-1} \\ 0 & x_q & x_{q-1} & \cdots & x_{q-G-2} \\ \vdots & \vdots & \vdots & \vdots & \vdots \\ 0 & 0 & 0 & 0 & x_q \end{bmatrix}. \tag{19}$$

where $q = M(N+\nu)$. When (18) is expressed in a more concise format, we get

$$\bar{\mathbf{y}}_D^{(1)} = \bar{\mathbf{X}}^{(1)} \mathbf{G}_{SD} + \mathbf{w}_D^{(1)}, \tag{20}$$

where $\bar{\mathbf{X}}^{(1)} = \left[\mathbf{X}, \mathbf{X}, \mathbf{X}^*, \mathbf{X}^*\right]$ and $\mathbf{G}_{SD} = \left[\mathbf{g}_{SD}^{(1)\dagger}, \mathbf{g}_{SD}^{(2)\dagger}, \mathbf{g}_{SD}^{(3)\dagger}, \mathbf{g}_{SD}^{(4)\dagger}\right]^\dagger$. Following a similar strategy, one can write $\bar{\mathbf{y}}_D^{(2)}$ as

$$\bar{\mathbf{y}}_D^{(2)} = \bar{\mathbf{X}}^{(2)} \mathbf{G}_{SRD} + \mathbf{w}_D^{(2)}, \tag{21}$$

where $\bar{\mathbf{X}}^{(2)} = \left[\mathbf{X}, \mathbf{X}, \mathbf{X}, \mathbf{X}, \mathbf{X}^*, \mathbf{X}^*, \mathbf{X}^*, \mathbf{X}^*\right]$ and $\mathbf{G}_{SRD} = \left[\mathbf{g}_{SRD}^{(1)\dagger}, \mathbf{g}_{SRD}^{(2)\dagger}, \cdots, \mathbf{g}_{SD}^{(8)\dagger}\right]^\dagger$. Here,

$$\mathbf{g}_{SRD}^{(1)} = \Delta \eta_S \eta_R \eta_D \mathbf{g}_{SR} \otimes \mathbf{g}_{RD}, \tag{22a}$$
$$\mathbf{g}_{SRD}^{(2)} = \Delta \mu_S^* \mu_R \eta_D \mathbf{g}_{SR}^* \otimes \mathbf{g}_{RD}, \tag{22b}$$
$$\mathbf{g}_{SRD}^{(3)} = \Delta^* \mu_S^* \eta_R^* \mu_D \mathbf{g}_{SR}^* \otimes \mathbf{g}_{RD}^*, \tag{22c}$$
$$\mathbf{g}_{SRD}^{(4)} = \Delta^* \eta_S \mu_R^* \mu_D \mathbf{g}_{SR} \otimes \mathbf{g}_{RD}^*, \tag{22d}$$
$$\mathbf{g}_{SRD}^{(5)} = \Delta \mu_S \eta_R \eta_D \mathbf{g}_{SR} \otimes \mathbf{g}_{RD}, \tag{22e}$$
$$\mathbf{g}_{SRD}^{(6)} = \Delta \eta_S^* \mu_R \eta_D \mathbf{g}_{SR}^* \otimes \mathbf{g}_{RD}, \tag{22f}$$
$$\mathbf{g}_{SRD}^{(7)} = \Delta^* \eta_S^* \eta_R^* \mu_D \mathbf{g}_{SR}^* \otimes \mathbf{g}_{RD}^*, \tag{22g}$$
$$\mathbf{g}_{SRD}^{(8)} = \Delta^* \mu_S \mu_R^* \mu_D \mathbf{g}_{SR} \otimes \mathbf{g}_{RD}^*. \tag{22h}$$

These structures allow us to estimate just two parameters, $\mathbf{G}_{SD}$ and $\mathbf{G}_{SRD}$, rather than the nine parameters of $\mathbf{g}_{SR}$, $\mathbf{g}_{SD}$, $\mathbf{g}_{RD}$, η_S, μ_S, η_R, μ_R, η_D, and μ_D. The ML assessments of $\mathbf{G}_{SD}$ and $\mathbf{G}_{SRD}$ are produced by optimizing the log-likelihood function as

$$\left[\hat{\mathbf{G}}_{SD}, \hat{\mathbf{G}}_{SRD}\right] = \arg \max_{\mathbf{G}_{SD},\mathbf{G}_{SRD}} \log \times \Pr\left(\overline{\mathbf{y}}_D^{(1)}, \overline{\mathbf{y}}_D^{(2)} \middle| \overline{\mathbf{X}}^{(1)}, \overline{\mathbf{X}}^{(2)}, \mathbf{G}_{SD}, \mathbf{G}_{SRD}\right), \tag{23}$$

where $\Pr(\circ|\triangleright)$ is defined as the probability density function of $\circ$ given $\triangleright$, and $\hat{\circ}$ represents the estimated value of $\circ$. Since $\overline{\mathbf{y}}_D^{(1)}$ and $\overline{\mathbf{y}}_D^{(2)}$ are independent vectors, we write

$$\Pr\left(\overline{\mathbf{y}}_D^{(1)}, \overline{\mathbf{y}}_D^{(2)} \middle| \overline{\mathbf{X}}^{(1)}, \overline{\mathbf{X}}^{(2)}, \mathbf{G}_{SD}, \mathbf{G}_{SRD}\right) = \Pr\left(\overline{\mathbf{y}}_D^{(1)} \middle| \overline{\mathbf{X}}^{(1)}, \mathbf{G}_{SD}\right) \Pr\left(\overline{\mathbf{y}}_D^{(2)} \middle| \overline{\mathbf{X}}^{(2)}, \mathbf{G}_{SRD}\right), \tag{24}$$

where

$$\Pr\left(\overline{\mathbf{y}}_D^{(1)} \middle| \overline{\mathbf{X}}^{(1)}, \mathbf{G}_{SD}\right) \propto \exp\left(\frac{-1}{\sigma_n^2} \left\|\overline{\mathbf{y}}_D^{(1)} - \overline{\mathbf{X}}^{(1)}\mathbf{G}_{SD}\right\|^2\right), \tag{25}$$

and

$$\Pr\left(\overline{\mathbf{y}}_D^{(2)} \middle| \overline{\mathbf{X}}^{(2)}, \mathbf{G}_{SRD}\right) \propto \exp\left(\frac{-1}{\sigma_n^2} \left\|\overline{\mathbf{y}}_D^{(2)} - \overline{\mathbf{X}}^{(2)}\mathbf{G}_{SRD}\right\|^2\right). \tag{26}$$

According to (23-26), the exact ML solution necessitates prior knowledge of the transmission matrices $\overline{\mathbf{X}}^{(1)}$ and $\overline{\mathbf{X}}^{(2)}$, which are typically unavailable. In such situations when nuisance parameters are present, the EM mechanism offers a solution that involves repeated iterations of the search for the ML estimates [29], [30]. The mechanism rotates between conducting an expectation step (E-step) and a maximization step (M-step) in each iteration. The E-step quantifies the expectation of the logarithmic likelihood of observed signal with respect to the conditional distribution of the unobserved data, given current estimates of the unknown parameters. The M-step optimizes the quantity previously derived in the E-step to obtain fresh estimates for the unknown parameters. The mathematical expression for the E-step at iteration ι is

$$\begin{aligned}
&\mathrm{U}\left([\mathbf{G}_{SD}, \mathbf{G}_{SRD}] \middle| \left[\hat{\mathbf{G}}_{SD}(\iota), \hat{\mathbf{G}}_{SRD}(\iota)\right]\right) \\
&= \mathrm{E}\left[\log \Pr\left(\overline{\mathbf{y}}_D^{(1)}, \overline{\mathbf{y}}_D^{(2)} \middle| \overline{\mathbf{X}}^{(1)}, \overline{\mathbf{X}}^{(2)}, \mathbf{G}_{SD}, \mathbf{G}_{SRD}\right) \middle| \overline{\mathbf{y}}_D^{(1)}, \overline{\mathbf{y}}_D^{(2)}, \hat{\mathbf{G}}_{SD}(\iota), \hat{\mathbf{G}}_{SRD}(\iota)\right] \\
&= \int_{\overline{\mathbf{X}}^{(1)},\overline{\mathbf{X}}^{(2)}} \log \Pr\left(\overline{\mathbf{y}}_D^{(1)}, \overline{\mathbf{y}}_D^{(2)} \middle| \overline{\mathbf{X}}^{(1)}, \overline{\mathbf{X}}^{(2)}, \mathbf{G}_{SD}, \mathbf{G}_{SRD}\right) \\
&\quad \times \Pr\left(\overline{\mathbf{X}}^{(1)}, \overline{\mathbf{X}}^{(2)} \middle| \overline{\mathbf{y}}_D^{(1)}, \overline{\mathbf{y}}_D^{(2)}, \hat{\mathbf{G}}_{SD}(\iota), \hat{\mathbf{G}}_{SRD}(\iota)\right) d\overline{\mathbf{X}}^{(1)} d\overline{\mathbf{X}}^{(2)},
\end{aligned} \tag{27}$$

where the expectation is carried out over the matrices $\overline{\mathbf{X}}^{(1)}$ and $\overline{\mathbf{X}}^{(2)}$. This leads us to a derivation of the M-step as

$$\left[\hat{\mathbf{G}}_{SD}(\iota+1), \hat{\mathbf{G}}_{SRD}(\iota+1)\right] = \arg \max_{\mathbf{G}_{SD},\mathbf{G}_{SRD}} \mathrm{U}\left([\mathbf{G}_{SD}, \mathbf{G}_{SRD}] \middle| \left[\hat{\mathbf{G}}_{SD}(\iota), \hat{\mathbf{G}}_{SRD}(\iota)\right]\right). \tag{28}$$

When we plug (24), (25), and (26) into (27) with leaving out the useless terms, we get

$$\begin{aligned}
&\mathrm{U}\left([\mathbf{G}_{SD}, \mathbf{G}_{SRD}] \middle| \left[\hat{\mathbf{G}}_{SD}(\iota), \hat{\mathbf{G}}_{SRD}(\iota)\right]\right) \\
&\propto 2\Re\left(\overline{\mathbf{y}}_D^{(1)\ddagger}\mathbf{A}_1\mathbf{G}_{SD}\right) - \mathbf{G}_{SD}^{\ddagger}\mathbf{A}_2\mathbf{G}_{SD} \\
&\quad + 2\Re\left(\overline{\mathbf{y}}_D^{(2)\ddagger}\mathbf{B}_1\mathbf{G}_{SRD}\right) - \mathbf{G}_{SRD}^{\ddagger}\mathbf{B}_2\mathbf{G}_{SRD},
\end{aligned} \tag{29}$$

where the superscript $\ddagger$ denotes the vector transpose conjugate of a vector, and

$$\mathbf{A}_1 = \int \overline{\mathbf{X}}^{(1)} \Pr\left(\overline{\mathbf{X}}^{(1)} \middle| \overline{\mathbf{y}}_D^{(1)}, \hat{\mathbf{G}}_{SD}(\iota)\right) d\overline{\mathbf{X}}^{(1)}, \tag{30a}$$

$$\mathbf{A}_2 = \int \overline{\mathbf{X}}^{(1)\ddagger}\overline{\mathbf{X}}^{(1)} \Pr\left(\overline{\mathbf{X}}^{(1)} \middle| \overline{\mathbf{y}}_D^{(1)}, \hat{\mathbf{G}}_{SD}(\iota)\right) d\overline{\mathbf{X}}^{(1)}, \tag{30b}$$

$$\mathbf{B}_1 = \int \overline{\mathbf{X}}^{(2)} \Pr\left(\overline{\mathbf{X}}^{(2)} \middle| \overline{\mathbf{y}}_D^{(2)}, \hat{\mathbf{G}}_{SRD}(\iota)\right) d\overline{\mathbf{X}}^{(2)}, \tag{30c}$$

$$\mathbf{B}_2 = \int \overline{\mathbf{X}}^{(2)\ddagger}\overline{\mathbf{X}}^{(2)} \Pr\left(\overline{\mathbf{X}}^{(2)} \middle| \overline{\mathbf{y}}_D^{(2)}, \hat{\mathbf{G}}_{SRD}(\iota)\right) d\overline{\mathbf{X}}^{(1)}. \tag{30d}$$

We revise the earlier estimates of $\mathbf{G}_{SD}$ and $\mathbf{G}_{SRD}$ by setting the derivative of (29) with respect to $\mathbf{G}_{SD}$ and $\mathbf{G}_{SRD}$ to zero as

$$\hat{\mathbf{G}}_{SD}(\iota+1) = \mathbf{A}_2^{-1}\mathbf{A}_1\overline{\mathbf{y}}_D^{(1)}, \tag{31a}$$

$$\hat{\mathbf{G}}_{SRD}(\iota+1) = \mathbf{B}_2^{-1}\mathbf{B}_1\overline{\mathbf{y}}_D^{(2)}, \tag{31b}$$

The following observations are worth taking into consideration.

- The question of how to actually determine the matrices of $\mathbf{A}_1$, $\mathbf{A}_2$, $\mathbf{B}_1$ and $\mathbf{B}_2$ in reality emerges next. It is indicated from (1) that

$$\mathrm{E}\left[x^{(m)}(n)\right] = \frac{1}{\sqrt{N}} \sum_{k=0}^{N-1} \mathrm{E}\left[d^{(m)}(k)\right] \exp(-j2\pi nk/N), \tag{32}$$

  where

$$\mathrm{E}\left[d^{(m)}(k)\right] = \sum_{\omega\in\Omega} \Pr\left(d^{(m)}(k) = \omega \mid \overline{\mathbf{y}}_D^{(1)}, \overline{\mathbf{y}}_D^{(2)}, \hat{\mathbf{G}}_{SD}(\iota), \hat{\mathbf{G}}_{SRD}(\iota)\right). \tag{33}$$

  Therefore, the *a posteriori* expectation of the matrix $\mathbf{X}$ shown in (19) can be constructed by replacing each element in the matrix with its corresponding *a posteriori* expectation computed in (32). Accordingly, one can easily construct the matrices of $\mathbf{A}_1$ and $\mathbf{B}_1$ as $\mathbf{A}_1 = \left[\tilde{\mathbf{X}}, \tilde{\mathbf{X}}, \tilde{\mathbf{X}}^*, \tilde{\mathbf{X}}^*\right]$ and $\mathbf{B}_1 = \left[\tilde{\mathbf{X}}, \tilde{\mathbf{X}}, \tilde{\mathbf{X}}, \tilde{\mathbf{X}}, \tilde{\mathbf{X}}^*, \tilde{\mathbf{X}}^*, \tilde{\mathbf{X}}^*, \tilde{\mathbf{X}}^*\right]$, where $\tilde{\mathbf{X}}$ is the *a posteriori* expectation of the matrix $\mathbf{X}$.
- In accordance with the widespread presumption that the data symbols are not correlated with one another, it is

possible to demonstrate that $\mathbf{A}_2$ and $\mathbf{B}_2$ can be approximately represented by $\mathbf{A}_1^{\ddagger}\mathbf{A}_1$ and $\mathbf{B}_1^{\ddagger}\mathbf{B}_1$, respectively.

- It is necessary to recalculate the *a posteriori* probability $\Pr\left(d^{(m)}(k)=\omega \mid \overline{\mathbf{y}}_D^{(1)}, \overline{\mathbf{y}}_D^{(2)}, \hat{\mathbf{G}}_{SD}(\iota), \hat{\mathbf{G}}_{SRD}(\iota)\right)$ after each time we make an adjustment to $\hat{\mathbf{G}}_{SD}(\iota)$ and $\hat{\mathbf{G}}_{SRD}(\iota)$. This necessitates restarting the channel decoder which adds substantial complexity to the data processing. We make use of the embedded estimation approach [30] to eliminate this complexity overhead. The channel decoder is not reset whenever the vectors $\hat{\mathbf{G}}_{SD}(\iota)$ and $\hat{\mathbf{G}}_{SRD}(\iota)$ are modified; rather, it retains the extrinsic and *a priori* probabilities that were calculated during the most recent iteration of the channel decoder. In such a setting, the proposed EM estimating algorithm's overhead is more affordable.
- The starting values for $\mathbf{G}_{SD}$ and $\mathbf{G}_{SRD}$ can be inferred using (31a) and (31b) by setting the matrices of the $\mathbf{A}_1$, $\mathbf{A}_2$, $\mathbf{B}_1$ and $\mathbf{B}_2$ to the contribution of the pilot symbols only.
- The computational difficulty of the offered estimator is quantified in terms of the number of floating-point-operations (fpos). By applying the same reasoning as in [17], [33], and [34], we can determine the necessary number of fpos, Λ, in each iteration as

$$\Lambda = 120GM(N+\nu). \tag{34}$$

We consider the numerical example where $G=10, M=20, N=128$, and $\nu=11$, and FPGA with a processing speed of ten Terafpos per second. Using (34), we obtain $\Lambda = 33792000$ fpos. This yields an execution period of 3.3792 μsec, which is fast enough for practical uses.

IV. PROPOSED DATA DETECTOR

In order to process the incoming signals, the destination divides them up into blocks of $N+\nu$ samples. The ν samples matching to the cyclic prefix are then eliminated, leaving N samples to be analyzed further. A N-point FFT operation is performed to transform the time-domain blocks into the frequency domain. After conducting an in-depth examination of (20) and (21), the outputs of the FFT unit at the kth bin of the mth block for both time slots are written as

$$R_1^{(m)}(k) = G_1(k)d^{(m)}(k) + G_2^{*}(-k)d^{(m)*}(-k) + W_1^{(m)}(k), \tag{35a}$$

$$R_2^{(m)}(k) = G_3(k)d^{(m)}(k) + G_4^{*}(-k)d^{(m)*}(-k) + W_2^{(m)}(k), \tag{35b}$$

where $W_1^{(m)}(k)$ and $W_2^{(m)}(k)$ are the corresponding noise factors and $G_i(k)$ is the frequency domain channel coefficient, $i=1,\cdots,4$. Utilizing (20) and (21), we can write $G_i(k)$ as the kth value returned by the FFT device used to process $\mathbf{g}_i$ as an input, where

$$\mathbf{g}_1 = \mathbf{g}_{SD}^{(1)} + \mathbf{g}_{SD}^{(2)}, \tag{36a}$$

$$\mathbf{g}_2 = \mathbf{g}_{SD}^{(3)} + \mathbf{g}_{SD}^{(4)}, \tag{36b}$$

$$\mathbf{g}_3 = \mathbf{g}_{SRD}^{(1)} + \mathbf{g}_{SRD}^{(2)} + \mathbf{g}_{SRD}^{(3)} + \mathbf{g}_{SRD}^{(4)}, \tag{36c}$$

$$\mathbf{g}_4 = \mathbf{g}_{SRD}^{(5)} + \mathbf{g}_{SRD}^{(6)} + \mathbf{g}_{SRD}^{(7)} + \mathbf{g}_{SRD}^{(8)}. \tag{36d}$$

We express (35a) and (35b) in a vector form as

$$\mathbf{R}^{(m)}(k) = \mathbf{G}(k)\mathbf{d}^{(m)}(k) + \mathbf{W}^{(m)}(k), \tag{37}$$

where $\mathbf{R}^{(m)}(k) = \left[R_1^{(m)}(k), R_1^{(m)}(k)\right]^{\dagger}$, $\mathbf{d}^{(m)}(k) = \left[d^{(m)}(k), d^{(m)*}(-k)\right]^{\dagger}$, and

$$\mathbf{G}(k) = \begin{bmatrix} G_1(k) & G_2^{*}(-k) \\ G_3(k) & G_3^{*}(-k) \end{bmatrix}. \tag{38}$$

The *a posteriori* probability of $\mathbf{d}^{(m)}(k)$ is expressed as

$$\Pr\left(\mathbf{d}^{(m)}(k)\,\middle|\,\mathbf{R}^{(m)}(k), \mathbf{G}(k)\right) \propto \exp\left(\frac{-1}{\sigma_n^2}\left\|\mathbf{R}^{(m)}(k) - \mathbf{G}(k)\mathbf{d}^{(m)}(k)\right\|^2\right)\Pr\left(\mathbf{d}^{(m)}(k)\right). \tag{39}$$

We assume each data symbol is identified by $Z=\log_2(\langle\Omega\rangle)$ bits, $d^{(m)}(k) = \mathcal{L}\left[b^{(m)}(k,0),\cdots,b^{(m)}(k,Z-1)\right]$, where $\mathcal{L}[\cdot]$ is the label function and $b^{(m)}(k,z)$ is the zth bit of the data symbol $d^{(m)}(k)$. Therefore, the bit metric $\lambda\left(b^{(m)}(k,z)=o\right)$, for $o=0,1$, is computed as [35] and [36]

$$\lambda\left(b^{(m)}(k,z)=o\right) = \sum_{\vartheta=F(b,z)}\ \sum_{d^{(m)*}(-k)\in\Phi} \times \Pr\left(\mathbf{d}^{(m)}(k)\,\middle|\,\mathbf{R}^{(m)}(k), \mathbf{G}(k), d^{(m)}(k)=\vartheta\right), \tag{40}$$

where

$$F(b,z) = \mathcal{L}\left\{\left[b^{(m)}(k,0),\cdots,b^{(m)}(k,Z-1)\right]\,\middle|\,b^{(m)}(k,z)=o\right\}. \tag{41}$$

The bit metrics are supplied to the decoder after de-interleaving to obtain the *a posteriori* probability of coded bits. After that, the probabilities are interleaved and sent to the data symbol *a posteriori* calculation unit. These probabilities are supplied as *a priori* information to the proposed estimator and detector algorithms, as shown in (31a), (31b), and (39), respectively. At the last iteration, the decoder uses the *a posteriori* probabilities of the transmitted bits to make hard decisions. Figure 3 portrays the conceptual block diagram of the suggested detection and estimation procedures.

V. SIMULATION RESULTS

We utilized Monte Carlo simulations in order to verify the efficacy of the offered estimation and detection approach. We investigated a coded wireless cooperative OFDM system with an AF relaying strategy. The following system parameters were used throughout simulations, unless explicitly specified differently in the text. A random interleaver and a half-rate convolutional code of a constraint length

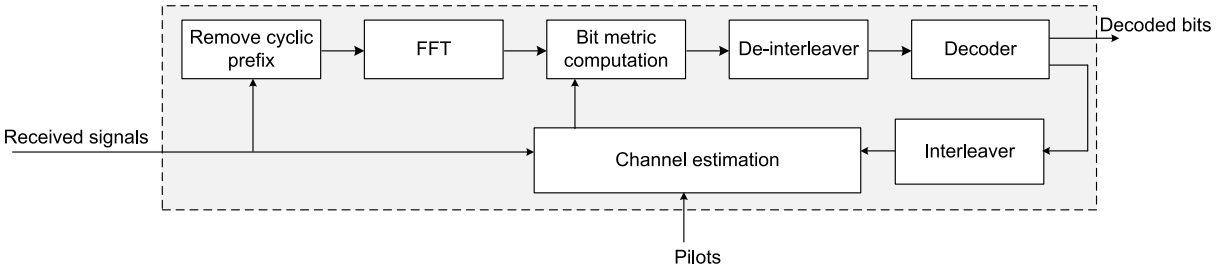

FIGURE 3. Conceptual block diagram of the proposed detection and estimation process.

of 7 and polynomials of 24 and 37 were taken into account for a bit-interleaved coded modulation transmission. Set-partition mapping was adopted to map coded bits onto 16-QAM modulated signals. Transmission frames of 1840 data symbols were produced. To accomplish preliminary channel estimation, a training sequence with a size of $T = 60$ symbols was attached to each frame. Each frame was divided into $M = 15$ blocks with no overlap. The blocks were revolutionized to OFDM symbols using an IFFT process with a length of $N = 124$ and a cyclic prefix of 8 samples. The connection between any two nodes was represented using seven elements, $g_{\varrho_1\varrho_2}(l)$, each of which was a complex zero-mean Gaussian random variable with an exponential power delay structure given as, [37] and [38]

$$g_{\varrho_1\varrho_2}(l) = \Phi_{\varrho_1\varrho_2} \exp(-l/10), \quad l = 0, \cdots, 6, \quad (42)$$

where ϱ_1 and $\varrho_2 \in \{S, R, D\}$, and $\Phi_{\varrho_1\varrho_2}$ has been picked in such a manner that would result in each sub-carrier having an average energy of $\Lambda_{\varrho_1\varrho_2}$. We set $\Lambda_{SD} = 1$, $\Lambda_{SR} = 1.8$, and $\Lambda_{RD} = 1.9$. The IQ parameters were $\rho_S = 0.92$, $\theta_S = 20^o$, $\rho_R = 0.91$, $\theta_R = 30^o$, and $\rho_D = 0.88$, $\theta_D = 26^o$.

Figure 4 depicts the bit error rate (BER) of the proposed detector as a function of the signal-to-noise ratio (SNR), whereas figure 5 displays the mean square error (MSE) of the proposed estimator. Figure 5 also offers the MSE of an estimator with entire awareness of all data symbols as a point of comparison. This creates a lower constraint on MSE performance. Furthermore, we include the MSE performance of the algorithms reported in [39] and [40]. The MSE results demonstrate that the suggested algorithm surpasses the reported ones due to its optimization for use with IQ settings. Figure 4 also shows the BER performance when complete information of CIRs between nodes and IQ parameters is assumed. As observed from the two figures, while the iteration process continues, MSE and BER performance continue to improve. After 8 cycles and high SNR values, the proposed detector and estimator attain the performance under ideal conditions of complete channel information and IQ parameters. The following is an explanation for this. In the first cycle, the offered detector's soft information is unreliable since the estimation procedure is based on a small number of pilots. The accuracy of the prediction and data detection, however, enhances with an increased number of cycles, since

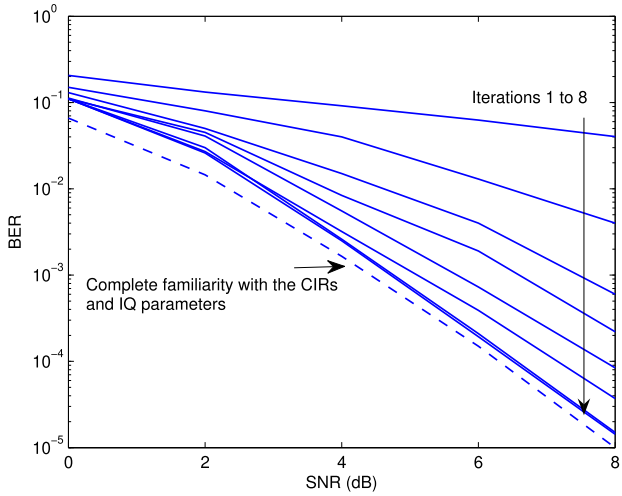

FIGURE 4. BER of the stated detector when used with the offered CIRs and IQ parameters estimator.

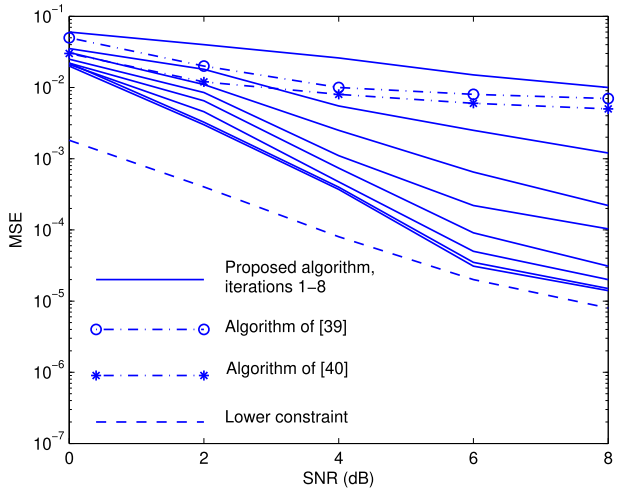

FIGURE 5. MSE performance of the computed CIRs along with IQ parameters versus SNR.

more information is used in comparison to the data-aided scenario.

Figure 6 presents a comparison of the BER performance of the proposed architecture with that of a variety of other systems. There is the scenario with perfect prediction and adjustment for an IQ mismatch, as well as the case with no

TABLE 1. The connection between the number of pilot symbols, BER, and iterations required to converge at SNR = 8 dB.

Number of pilot symbols	BER	Minimum number of iterations to converge
20	0.2	∞
40	0.05	20
60	$(1.2)\,10^{-5}$	8
80	$(1.18)\,10^{-5}$	7

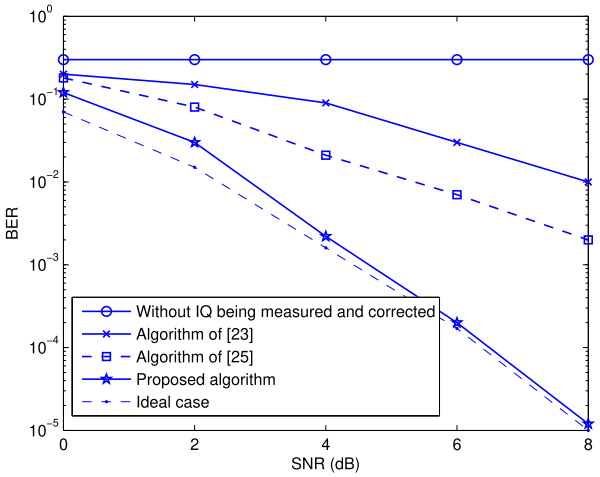

FIGURE 6. BER performance comparison of different systems.

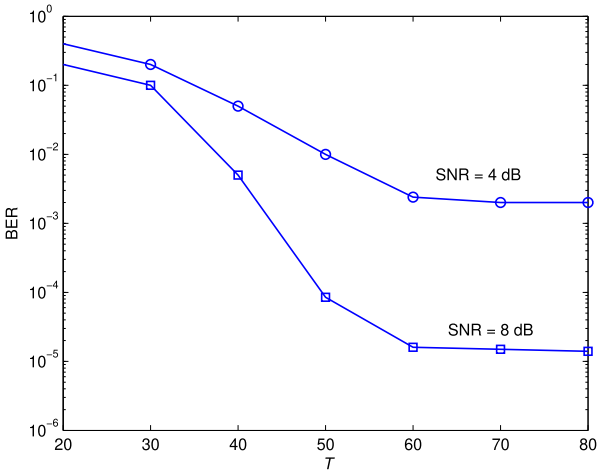

FIGURE 8. Impact of the number of pilot systems on the system performance.

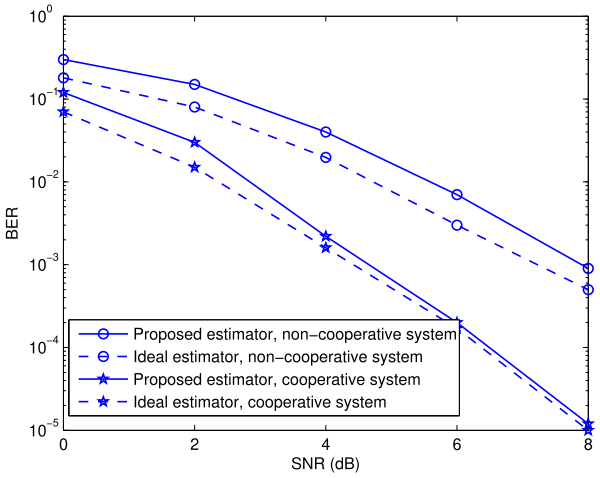

FIGURE 7. BER of the cooperative and non-cooperative systems with the offered CIRs and IQ parameters estimator.

IQ compensation at all. As can be seen, IQ disparity will result in an inadequate BER performance if not adjusted for. Evidently, the offered process has a BER performance that is substantially better than that described in [23] and [25], and it also comes within 1 dB of the ideal performance.

Conventional non-cooperative OFDM broadcasts may also benefit from the offered approach. The channel coefficients between the relay and the destination need only be wiped out. In this instance, however, the proposed detector operates identically to the standard one. Figure 7 demonstrates a comparison between the BER accuracy of the proposed AF-OFDM system and the non-cooperative OFDM system linked to the proposed estimator at iteration 8. Findings show that the cooperative system is much superior to the non-cooperative one. This is due to the fact that the cooperative system makes optimal use of diversity gain by sending signals via both direct and relay links.

An effective initiation is well-known to be crucial to EM-based algorithms. Using SNR = 8 dB and SNR = 4 as examples, Figure 8 displays the BER performance of the proposed detector and estimator as a function of T. It is clear that the suggested estimator has a high convergent threshold of more than 60 pilots. It's important to note that the bare minimum of pilots needed to provide reliable first estimates may vary based on the specifics of the system and the links. Our estimating technique may be used in practice over a wide range of system and connection characteristics to determine the bare minimum of pilots necessary to achieve all the specified criteria. This information is then utilized in the hardware implementation using look up tables. The designer may also choose a large enough sample of pilots at random to cover a broad variety of system and connection settings.

The number of pilot symbols, BER, and number of iterations required to converge at SNR = 8 dB are all shown in Table 1. A higher number of pilots leads to a lower BER and fewer iterations to convergence, as shown by the findings. Relying on a limited set of pilots to achieve satisfactory BER performance is futile, even after many iterations. In addition, a large number of pilots leads to perfect BER performance with few iterations.

Figure 9 displays the BER performance of the offered approach over a wide range of SNR for a family of QAM modulation formats with orders of 4, 16, 64, and 128 at iteration 8. An increase in BER is noticed when a higher-order

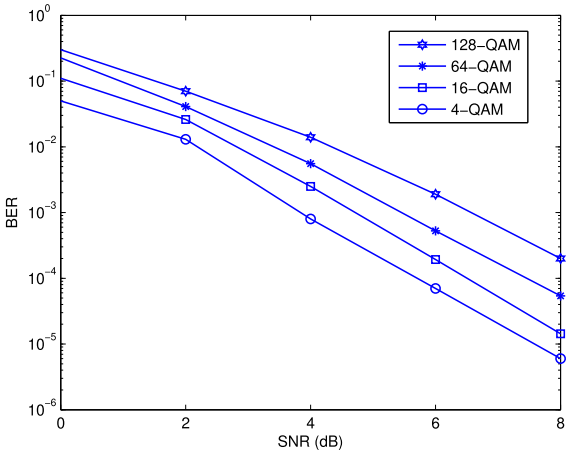

FIGURE 9. Influence of modulation order on the BER performance.

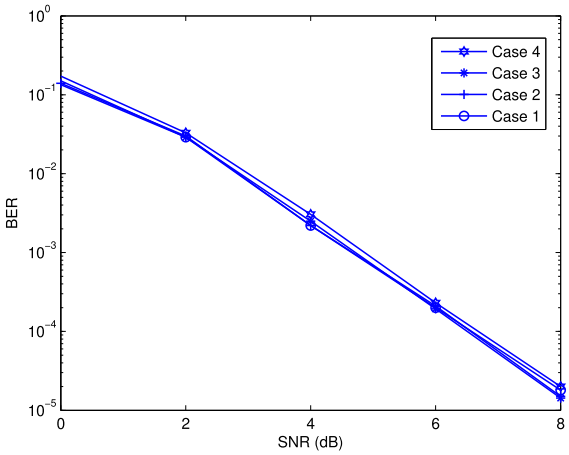

FIGURE 10. BER performance of the proposed designed at various cases of IQ parameters.

modulation form is adopted. This is due to the fact that the soft information results of the channel decoder are less trustworthy as a consequence of employing a higher-order modulation scheme, which in turn has a detrimental impact on the BER performance.

The previous findings were acquired for specific values of IQ at the source, relay, and destination nodes, as explained above. We run additional simulations to demonstrate how well the proposed approach works in a variety of IQ settings. The following are four different IQ cases to examine.

- Case 1: $\rho_S = 0.92, \theta_S = 20^o, \rho_R = 0.91, \theta_R = 30^o,$ and $\rho_D = 0.88, \theta_D = 26^o,$
- Case 2: $\rho_S = 0.95, \theta_S = 15^o, \rho_R = 0.93, \theta_R = 20^o,$ and $\rho_D = 0.98, \theta_D = 16^o,$
- Case 3: $\rho_S = 0.89, \theta_S = 6^o, \rho_R = 0.86, \theta_R = 10^o,$ and $\rho_D = 0.95, \theta_D = 8^o,$
- Case 4: $\rho_S = 0.97, \theta_S = 12^o, \rho_R = 0.9, \theta_R = 5^o,$ and $\rho_D = 0.91, \theta_D = 14^o.$

The preceding numerical values of IQ parameters were chosen at random to cover a wide variety of different conceivable setups. Figure 10 illustrates the BER performance of the proposed algorithm for the stated cases. The findings show that there are no discernible variations among the four cases. This is because the proposed structure combines the channel impulse responses with the values of all IQ parameters, yielding estimates for two equivalent parameters. This provides an evidence that the offered solution is powerful.

VI. CONCLUSION

We offered a revolutionary EM-based approach for the issue of inferring the channel impulse responses, as well as the source, relay, and destination IQ mismatch parameters for AF-OFDM systems. The proposed approach made use of the soft information that was being supplied by the channel decoder in order to improve the estimations, without the need for an extra equalizer. It has the advantage of interacting with any channel decoder that can determine the *a posteriori* probability of the information symbols. Instead of using numerous separate methods to determine the IQ mismatch parameters at the source, relay, and destination, as well as the CIRs between the aforementioned nodes, the suggested estimation technique can accomplish all of these activities in a single pass. We also showed how to utilize the estimated parameters to conduct data detection. According to the simulation findings, the BER performance of the suggested detector, when used in combination with the proposed estimate technique, is very near to the BER of the ideal scenario in which all of the parameters are known in advance, with superiority over the conventional ones.

ACKNOWLEDGMENT

The authors would like to acknowledge the support of Prince Sultan University for paying the Article Processing Charges (APC) of this publication.

REFERENCES

[1] B. Bossy, P. Kryszkiewicz, and H. Bogucka, "Energy-efficient OFDM radio resource allocation optimization with computational awareness: A survey," *IEEE Access*, vol. 10, pp. 94100–94132, 2022.
[2] S. D. Liyanaarachchi, T. Riihonen, C. B. Barneto, and M. Valkama, "Optimized waveforms for 5G–6G communication with sensing: Theory, simulations and experiments," *IEEE Trans. Wireless Commun.*, vol. 20, no. 12, pp. 8301–8315, Dec. 2021.
[3] T. Kebede, Y. Wondie, J. Steinbrunn, H. B. Kassa, and K. T. Kornegay, "Multi-carrier waveforms and multiple access strategies in wireless networks: Performance, applications, and challenges," *IEEE Access*, vol. 10, pp. 21120–21140, 2022.
[4] U. Singh, A. Dua, S. Tanwar, N. Kumar, and M. Alazab, "A survey on LTE/LTE—A radio resource allocation techniques for machine-to-machine communication for B5G networks," *IEEE Access*, vol. 9, pp. 107976–107997, 2021.
[5] D. F. Carrera, C. Vargas-Rosales, D. Zabala-Blanco, N. M. Yungaicela-Naula, C. A. Azurdia-Meza, M. Marey, and A. D. Firoozabadi, "Novel multilayer extreme learning machine as a massive MIMO receiver for millimeter wave communications," *IEEE Access*, vol. 10, pp. 58965–58981, 2022.
[6] M. Huang, J. Chen, and S. Feng, "Synchronization for OFDM-based satellite communication system," *IEEE Trans. Veh. Technol.*, vol. 70, no. 6, pp. 5693–5702, Jun. 2021.
[7] S. Tan, Y. Ren, J. Yang, and Y. Chen, "Commodity WiFi sensing in ten years: Status, challenges, and opportunities," *IEEE Internet Things J.*, vol. 9, no. 18, pp. 17832–17843, Sep. 2022.

[8] Y. Liu, J. Yi, X. Wan, Y. Rao, and J. Shen, "PAPR reduction of OFDM waveform in integrated passive radar and communication systems," *IEEE Sensors J.*, vol. 22, no. 17, pp. 17307–17317, Sep. 2022.

[9] X. Zhang, Y. Xia, C. Li, L. Yang, and D. P. Mandic, "Complex properness inspired blind adaptive frequency-dependent I/Q imbalance compensation for wideband direct-conversion receivers," *IEEE Trans. Wireless Commun.*, vol. 19, no. 9, pp. 5982–5992, Sep. 2020.

[10] A. Shehata, P. Mary, and M. Crussiere, "Analysis of compressing PAPR-reduced OFDM IQ samples for cloud radio access network," *IEEE Trans. Broadcast.*, vol. 68, no. 3, pp. 765–779, Sep. 2022.

[11] A. Mohammadian, C. Tellambura, and G. Y. Li, "Deep learning LMMSE joint channel, PN, and IQ imbalance estimator for multicarrier MIMO full-duplex systems," *IEEE Wireless Commun. Lett.*, vol. 11, no. 1, pp. 111–115, Jan. 2022.

[12] M. Sandell, E. Tsimbalo, S. Jardak, D. Uchida, K. Akita, D. Yoda, T. Kawaguchi, and M. Sano, "Estimation of wideband IQ imbalance in MIMO OFDM systems with CFO," *IEEE Trans. Wireless Commun.*, vol. 20, no. 9, pp. 5821–5830, Sep. 2021.

[13] J. Li, T. Xin, B. He, and W. Li, "IQ symbols processing schemes with LSTMs in OFDM system," *IEEE Access*, vol. 10, pp. 70737–70745, 2022.

[14] A. Mohammadian and C. Tellambura, "RF impairments in wireless transceivers: Phase noise, CFO, and IQ imbalance—A survey," *IEEE Access*, vol. 9, pp. 111718–111791, 2021.

[15] Y. Xiao, X. Jin, Y. Shen, and Q. Guan, "Joint relay selection and adaptive modulation and coding for wireless cooperative communications," *IEEE Sensors J.*, vol. 21, no. 22, pp. 25508–25516, Nov. 2021.

[16] N. Biswas, Z. Wang, L. Vandendorpe, and H. Mirghasemi, "On joint cooperative relaying, resource allocation, and scheduling for mobile edge computing networks," *IEEE Trans. Commun.*, vol. 70, no. 9, pp. 5882–5897, Sep. 2022.

[17] M. Marey, H. Mostafa, O. A. Dobre, and M. H. Ahmed, "Data detection algorithms for BICM alternate-relaying cooperative systems with multiple-antenna destination," *IEEE Trans. Veh. Technol.*, vol. 65, no. 5, pp. 3802–3807, Jun. 2016.

[18] J. Zhou, S. Dang, B. Shihada, and M.-S. Alouini, "Power allocation for relayed OFDM with index modulation assisted by artificial neural network," *IEEE Wireless Commun. Lett.*, vol. 10, no. 2, pp. 373–377, Feb. 2021.

[19] Y. Jin, X. Li, G. Lv, M. Zhao, and Y. Jin, "Secure resource allocation for cooperative OFDMA system with untrusted AF relaying," *IEEE Access*, vol. 9, pp. 156818–156830, 2021.

[20] S. Dang, J. Zhou, B. Shihada, and M.-S. Alouini, "Relay assisted OFDM with subcarrier number modulation in multi-hop cooperative networks," *IEEE Wireless Commun. Lett.*, vol. 9, no. 11, pp. 1869–1873, Nov. 2020.

[21] E. Balti and B. K. Johnson, "On the joint effects of HPA nonlinearities and IQ imbalance on mixed RF/FSO cooperative systems," *IEEE Trans. Commun.*, vol. 69, no. 11, pp. 7879–7894, Nov. 2021.

[22] A. Gouissem, R. Hamila, and M. O. Hasna, "Outage performance of cooperative systems under IQ imbalance," *IEEE Trans. Commun.*, vol. 62, no. 5, pp. 1480–1489, May 2014.

[23] M. Mokhtar, A. Gomaa, and N. Al-Dhahir, "OFDM AF relaying under I/Q imbalance: Performance analysis and baseband compensation," *IEEE Trans. Commun.*, vol. 61, no. 4, pp. 1304–1313, Apr. 2013.

[24] J. Wang, H. Yu, Y. Wu, F. Shu, J. Wang, R. Chen, and J. Li, "Pilot optimization and power allocation for OFDM-based full-duplex relay networks with IQ-imbalances," *IEEE Access*, vol. 5, pp. 24344–24352, 2017.

[25] J. Li, M. Matthaiou, and T. Svensson, "I/Q imbalance in AF dual-hop relaying: Performance analysis in Nakagami-m fading," *IEEE Trans. Commun.*, vol. 62, no. 3, pp. 836–847, Mar. 2014.

[26] J. Li, M. Matthaiou, and T. Svensson, "I/Q imbalance in two-way AF relaying," *IEEE Trans. Wireless Commun.*, vol. 62, no. 7, pp. 2271–2285, Jul. 2014.

[27] M. Marey, "Solving IQ mismatch problem for two-path successive relaying OFDMA uplink systems with direct conversion transceivers," *IEEE Wireless Commun. Lett.*, vol. 8, no. 1, pp. 33–36, Feb. 2019.

[28] M. Marey, "Soft-information aided channel estimation with IQ imbalance for alternate-relaying OFDM cooperative systems," *IEEE Wireless Commun. Lett.*, vol. 7, no. 3, pp. 308–311, Jun. 2018.

[29] X. Feng, J. Wang, X. Kuai, M. Zhou, H. Sun, and J. Li, "Message passing-based impulsive noise mitigation and channel estimation for underwater acoustic OFDM communications," *IEEE Trans. Veh. Technol.*, vol. 71, no. 1, pp. 611–625, Jan. 2022.

[30] J. Rodriguez-Fernandez, "Joint synchronization and compressive channel estimation for frequency-selective hybrid mmWave MIMO systems," *IEEE Trans. Wireless Commun.*, vol. 21, no. 1, pp. 548–562, Jan. 2022.

[31] F. Launay and A. Perez, *LTE Advanced Pro: Towards the 5G Mobile Network*. Hoboken, NJ, USA: Wiley, 2019.

[32] S. S. Ikki and S. Aissa, "Performance analysis of two-way amplify-and-forward relaying in the presence of co-channel interferences," *IEEE Trans. Commun.*, vol. 60, no. 4, pp. 933–939, Apr. 2012.

[33] H. Mostafa, M. Marey, M. H. Ahmed, and O. A. Dobre, "Decoding techniques for alternate-relaying BICM cooperative systems," *EURASIP J. Wireless Commun. Netw.*, vol. 2013, p. 236, Sep. 2013.

[34] H. Mostafa, M. Marey, M. H. Ahmed, and O. A. Dobre, "Simplified maximum-likelihood detectors for full-rate alternate-relaying cooperative systems," *IET Commun.*, vol. 7, no. 17, pp. 1899–1906, Nov. 2013.

[35] M. Marey, M. Guenach, and H. Steendam, "Code-aided channel tracking and frequency offset-phase noise elimination for multicarrier systems," *IEEE Signal Process. Lett.*, vol. 15, pp. 657–660, 2008.

[36] M. Marey and H. Mostafa, "Code-aided modulation classification algorithm for multiuser uplink SC-FDMA systems," *IEEE Wireless Commun. Lett.*, vol. 10, no. 5, pp. 1023–1027, May 2021.

[37] E. Bedeer, M. Marey, O. Dobre, and K. Baddour, "Adaptive bit allocation for OFDM cognitive radio systems with imperfect channel estimation," in *Proc. IEEE Radio Wireless Symp.*, Jan. 2012, pp. 359–362.

[38] M. Marey and H. Steendam, "The effect of narrowband interference on frequency ambiguity resolution for OFDM," in *Proc. IEEE Veh. Technol. Conf.*, Sep. 2006, pp. 1–5.

[39] S. Abdallah, A. I. Salameh, and M. Saad, "Spectrum efficient joint frequency offset and channel estimation for time-asynchronous amplify-and forward two-way relay networks," *IEEE Access*, vol. 7, pp. 71972–71985, 2019.

[40] S. M. S. Sadough and Z. Chamideh, "Efficient variational Bayesian method for joint channel estimation and signal detection in OFDM-based AF relay networks," *IEEE Commun. Lett.*, vol. 19, no. 10, pp. 1786–1789, Oct. 2015.

MOHAMED MAREY (Senior Member, IEEE) received the M.Sc. degree in electrical engineering from Menoufia University, Egypt, in 1999, and the Ph.D. degree in electrical engineering from Ghent University, Belgium, in 2008. From 2009 to 2014, he was a Research Associate and a Visiting Professor with the Faculty of Engineering and Applied Science, Memorial University, Canada. He is currently a Full Professor with the Faculty of Electronic Engineering, Menoufia University. He is on a sabbatical leave in order to join Prince Sultan University, Saudi Arabia, as a Research Laboratory Leader of the Smart Systems Engineering Laboratory. He authored the book *Multi-Carrier Receivers in the Presence of Interference: Overlay Systems* (VDM Publishing House Ltd., 2009) and more than100 scientific papers published in international journals and conferences. His research interests include wireless communications and digital signal processing, with a particular focus on smart antennas, cooperative communications, signal classification for cognitive radio systems, synchronization and channel estimation, multiple-input multiple-output antenna systems, multi-carrier systems, and error correcting codes. He was a recipient of the Young Scientist Award from the International Union of Radio Science, in 1999. He serves as an Editor for the IEEE Open Journal of the Communications Society.

HALA MOSTAFA (Member, IEEE) received the Ph.D. degree in electrical engineering from the Faculty of Engineering and Applied Science, Memorial University, Canada, in 2014. From 2014 to 2015, she was a Research Scientist at Memorial University. She is currently an Assistant Professor with the Information Technology Department, College of Computer and Information Sciences, Princess Nourah bint Abdulrahman University, Riyadh, Saudi Arabia. Her research interests include wireless communications, with a particular focus on smart antennas and wireless sensor networks.